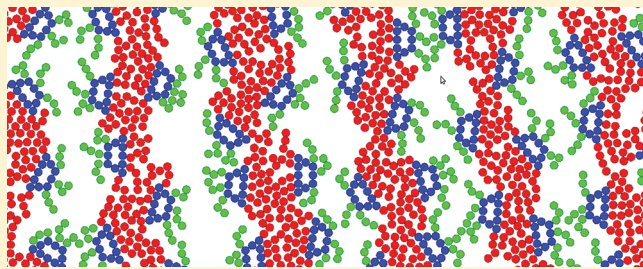


Solvent-Free Model for Self-Assembling Amphiphilic Cyclodextrins. An Off-Lattice Monte Carlo Approach in Two Dimensions

Alessandro Patti,* Roland Ramsch, and Conxita Solans Marsà

Institute of Advanced Chemistry of Catalonia (IQAC-CSIC) and CIBER de Bioingeniería, Biomateriales y Nanomedicina (CIBER-BBN), C/Jordi Girona, 18-26-08034 Barcelona, Spain

ABSTRACT: By performing off-lattice Monte Carlo simulations in a two-dimensional space, we investigate the aggregation behavior of model Bouquet-shaped amphiphilic cyclodextrins. These molecules are able to self-assemble into a variety of supramolecular structures, such as micelles, vesicles, and long double-layered filaments. At high packing fractions, inverted micellar phases and lamellar liquid crystals have also been observed. Despite the number of approximations and restrictions imposed in our model, where the solution degrees of freedom are kept implicit and only the main physicochemical details are considered, we are able to reproduce the self-assembling behavior of amphiphilic cyclodextrins in its essential and most characteristic picture. The calculations of the cluster size distribution, density profiles, and radial distribution functions permit the characterization of the aggregates formed in the self-assembly process.



I. INTRODUCTION

Cyclodextrins (CDs) are cyclic oligosaccharides consisting of 6 (α -), 7 (β -), or 8 (γ -CDs) units of dextrose bonded to each other and forming a truncated-cone-shaped cavity. Primary and secondary hydroxyl groups are incorporated respectively on the narrower and wider rims of this cavity. Although their discovery dates back to the end of the 19th century,¹ CDs achieved a deeper scientific attention only in the past four decades, when promising applications in the pharmaceutical,^{2,3} agrochemical,^{4–7} food,⁸ and cosmetic industries,⁹ based on the encapsulation of guest molecules, were extensively investigated.^{10–12} The inner cavity delimited by the truncated cone is not particularly lipophilic, but significantly less hydrophilic than the surrounding aqueous solution. By contrast, the external surface is hydrophilic enough to provide CDs a given degree of solubility in water. Thanks to this regioselective behavior, CDs behave as empty capsules whose inner cavity can include a broad selection of apolar guest molecules, thus forming the so-called inclusion complexes. This remarkable ability makes them suitable carriers in solubilization, encapsulation, transport, and delivery of bioactive molecules and drugs.^{2,3,13,14} Moreover, by acting as molecular cages, CDs can also preserve guest molecules from chemical degradation.¹⁵

However, because of the weak nature of the host–guest interactions upon dilution in water, the drug-transport efficiency of native CDs is inadequate in many practical cases.¹⁶ In order to obviate such an undesired limitation, there has been a deep scientific and technological interest in implementing an effective strategy for chemically modifying the CDs structure.^{17–19} Many different chemically modified CDs have been synthesized not only to promote their use as drug delivery systems but also to enhance their interactions with biological systems, such as membranes, and to use them as building

blocks for supramolecular self-assembling structures.¹⁷ To this end, several amphiphilic cyclodextrins (ACDs), such as lollipop,²⁰ cup-and-ball,²¹ Medusa-like,^{22,23} bouquet^{19,24,25} and skirt-shaped ACDs,^{26–28} have been synthesized by grafting hydrocarbon chains of various length on one or both sides of the cavity of native CDs. In particular, lollipops and cup-and-ball molecules are monosubstituted CDs including only one aliphatic chain grafted on the narrow side of the cavity.²⁹ In cup-and-ball CDs, the end of this aliphatic chain incorporates a bulky lipophilic group preventing the chain from entering the cavity.³⁰ The remaining structures are polysubstituted CDs: Medusa-like and skirt-shaped ACDs are obtained by grafting hydrocarbon chains to all the primary and secondary hydroxyl groups of the native CDs, respectively. Bouquet-shaped ACDs contain hydrocarbon chains on both sides of the asymmetric torus-shaped cavity.³¹

Monte Carlo (MC) and molecular dynamics (MD) simulation studies on native and modified CDs have been a powerful tool for a deeper comprehension of these molecules at the molecular level. Most of the investigations explored the hydration of native CDs, with special focus on the amount of water molecules which can be accommodated inside the lipophilic cavity and the corresponding interaction strength.^{32–39} Very recently, the hydration behavior of β -CDs has also been analyzed in ethanol, methanol, and mixtures of these solvents with water.⁴⁰ According to these studies, the average number of encapsulated water molecules, which strongly depends on several physicochemical properties, oscillates between two and five in β -CDs. This number increases with the size of the inner diameter of the cavity as observed

Received: December 24, 2011

Revised: February 10, 2012

Published: February 13, 2012

experimentally^{41,42} and confirmed by MD simulations.³⁶ Cezard et al. published detailed MD simulation results on the performance of several force fields for the description of geometrical, structural, and dynamic properties of solvated CDs and addressed many intriguing aspects related to hydrogen bonding,⁴³ such as the flip-flop phenomenon.⁴⁴ Interesting studies have also been reported on the mobility of several CD-based inclusion complexes.^{45–48}

Because of the molecular size and intrinsic complexity of CDs and derivatives, atomistic models cannot easily describe their self-assembly in supramolecular structures, as simulations would be too computationally demanding to reach any definitive result with current computing capabilities. Despite these substantial limitations, it is worth mentioning here two recent stimulating works on the aggregation of CDs via atomistic MD simulations. Cai and co-workers investigated the ability of cholesteryl-functionalized CDs to form spherical core–shell micelles for the design of promising drug carriers.⁴⁹ As these same authors pointed out, the complexity of modeling micellization allowed to observe only the self-assembly of small aggregates over the time scale considered (100 ns); larger aggregates would need longer sampling for equilibration as their shape and size deviate from those observed in experiments. Piñeiro and co-workers studied the aggregation of some tens of native α -CD molecules in water and at the water/air interface, with particular focus on their aggregation behavior when sodium dodecyl sulfate (SDS) is added.⁵⁰ In their 20 ns MD simulations, these authors showed that the presence of SDS into the α -CD cavity promotes the formation of a stable film of oriented self-assembled nanotubes whose building blocks are α -CD dimers (α -CD₂) and α -CD₂–SDS₁ complexes.

In both works, the atomistic representation of the solute(s) and solvent restricts the study to a short time scale and to a limited number of CDs molecules, hence precluding the chance to investigate long-range ordered phases and their periodical arrangement. To this end, one should introduce a number of approximations and assumptions, by coarse-graining the original system, that aim to simplify the physicochemical properties of the building blocks to only few important details. As a consequence, this makes the model less realistic, and a direct quantitative comparison with experiments is, in many cases, not feasible. Despite these unquestionable drawbacks, coarse-grained models can be of fundamental relevance to investigate the physics behind the aggregation behavior of many amphiphilic systems and thus to understand their equilibrium and/or dynamic behavior as a result of the most significant factors.

To the best of our knowledge, the present paper constitutes the first attempt to study, in the limits imposed by our simple coarse-grained model, the supramolecular self-assembling behavior of model ACDs, starting from a completely random initial configuration. To this aim, we model bouquet-shaped ACDs and perform MC simulations in a two-dimensional (2D) continuum space. Lattice and off-lattice MC simulations have extensively been applied to analyze the phase and aggregation behavior of a wide variety of amphiphilic systems in soft matter science, from simple^{51–58} to more complex^{59–63} model molecules. In our off-lattice MC simulations, we keep implicit the solution degrees of freedom, which implies to assume the presence of the solvent only in the effective interactions established between amphiphilic molecules. The effect of the interactions that the molecules of the solute would establish, in a more realistic scenario, with those of an explicit model

solvent, can be still taken into account by incorporating suitable phenomenological parameters, as previously proposed in the study of model ionic and nonionic surfactants.⁵¹ Although a number of details have to be neglected, a solvent-free model permits to reduce the computational time and hence to manage denser systems, while maintaining the focus on the key factors causing self-aggregation: (i) the attraction between lipophilic chains to avoid contact with the media and (ii) the repulsion between the hydrophilic chains.

To further simplify the model system and thus reduce the computational time to sample the configurational space, we decided to run our simulations in two dimensions. Obviously, this choice represents a crucial simplification of the problem: not only are we reducing three-dimensional (3D) molecules to their coarse-grained projection on a 2D space, but we are also constraining them to rotate and translate just in this space. Although these approximations make our model molecules less realistic than a 3D coarse-grained representation and much less realistic than a 3D atomistic one, they provide the unquestionable advantage of cutting down the significant number of interaction sites by keeping the essence of the above-mentioned factors promoting self-assembly. As a consequence, we stress that any comparison between the results stemming from our simulations and the experimental observations should be assessed on a mere qualitative basis. In the limits of these considerations, the present work aims to delineate the tendency of coarse-grained model ACDs to behave as building blocks for the formation of self-assembling supramolecular structures.

II. MODEL

As already pointed out above, the continuum model proposed here is relatively simple but still able to grasp the key factors leading to the self-aggregation of 2D bouquet-shaped ACDs. Each model molecule of ACDs consists of $N = 39$ connected beads, of which 10 constitute the truncated-cone-shaped cavity, and the remaining ones make up the hydrocarbon chains attached to the narrow and wide rims. The three chains linked to the narrow rim are significantly less lipophilic than the five chains incorporated into the opposite rim of the cavity. This difference gives the molecules an amphiphilic nature and permits their mutual self-aggregation. For the sake of concision, the less lipophilic chains will be denoted as hydrophilic chains throughout this paper. A model ACD contains 20 lipophilic and 9 hydrophilic beads, being equally distributed in 5 and 3 linear chains, respectively. The cavity, hydrophilic, and lipophilic beads will be indicated by C, H, and L, respectively. All the beads have the same diameter σ . The central cavity has a trapezoidal shape, representing the central longitudinal section of a truncated-cone-shaped cavity of a cyclodextrin molecule. Details can be observed in Figure 1, where a representation of a model 2D bouquet-shaped ACD is given.

The cavity of the ACDs behaves as a rigid body in a 2D space: it can rotate and/or translate, but its beads maintain their relative distances. We assume that the mutual interactions between these beads (C–C interactions) and those between them and any other bead in the system (C–H and C–L interactions) are hard-core interactions, and the corresponding potential reads

$$U_{ij}^{\text{HC}} = \begin{cases} \infty & r_{ij} \leq \sigma \\ 0 & r_{ij} > \sigma \end{cases} \quad (1)$$

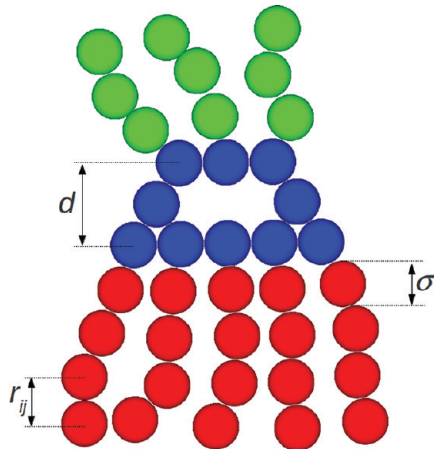


Figure 1. Model of a 2D bouquet-shaped ACD showing three hydrophilic arms of three beads each (green), five lipophilic arms of four beads each (red), and a central trapezoidal cavity with ten beads (blue). r_{ij} is the generic distance between two bonded beads, σ the bead diameter, and $d = 2\sigma \sin(\pi/3)$ the distance between the rims of the central cavity.

where U_{ij}^{HC} is the hard-core potential and r_{ij} the distance between beads i and j . Equation 1 is valid only if at least one of the two beads i or j belongs to the central cavity.

All the beads belonging to a given chain may move independently, being constrained to stay connected to each other by bond length and bond bending energy terms. Bonded and nonbonded interactions give the final shape of the total soft potential energy. A truncated and shifted Lennard-Jones (LJ) potential describes the nonbonded interactions due to the van der Waals forces. Mapping out the intermolecular interactions via a bare LJ potential has been of wide application in the past 20 years.^{51,64–68} The potential reads

$$U_{ij}^{\text{LJ}} = \begin{cases} 4\epsilon \left[\left(\frac{\sigma}{r_{ij}} \right)^{12} - \left(\frac{\sigma}{r_{ij}} \right)^6 \right] - U_0(R_c) & r_{ij} \leq R_c \\ 0 & r_{ij} > R_c \end{cases} \quad (2)$$

where U_{ij}^{LJ} is the LJ potential, R_c the cutoff radius, and ϵ the depth of the potential well. The term $U_0(R_c)$ makes the LJ potential vanish at $r_{ij} = R_c$ and beyond. We use ϵ and σ as energy and length units, respectively. The amphiphilic behavior of the ACDs is modeled by defining two different values of R_c , as previously proposed to investigate the micellization behavior of linear surfactants in solvent-free systems.^{51,67,69–74} More specifically, $R_c = 2^{1/6}\sigma$ to reproduce the effective H–H or H–L repulsions, whereas $R_c = 2.5\sigma$ to describe the attractive L–L interactions.

The interaction strength ϵ in the LJ potential function is a crucial phenomenological parameter for our coarse-grained model. Here, we would like to clarify its role for a better understanding of the results reported in section IV. From a strict mathematical point of view, ϵ is the depth of the potential well describing the nonbonded interactions (see eq 2). To fully understand its physical meaning, one should bear in mind that in our model the solvent is only implicitly assumed. If the solvent was explicitly modeled, the tendency to form aggregates to shield the lipophilic chains from the contact with the media would increase with its polarity. In water, for instance, above

the critical micellar concentration, amphiphiles can form micelles, but in a less polar media the same molecules might persist in their monomeric state even at relatively high concentrations. As a consequence of this self-assembly, the lipophilic chains cluster together as if their mutual interaction had become stronger. Therefore, by changing the strength of interactions between nonbonded beads and, more precisely, by increasing the attractions between the lipophilic ones, the resulting scenario would virtually be analogous to that of a system where the solvent polarity is higher. In other words, if the aim is to analyze the aggregation behavior of amphiphilic molecules in solvents of different polarity, this can be accomplished by properly tuning the interaction between the lipophilic beads, that is ϵ , as previously done in a number of solvent-free models.^{51,67,69–74} In order to choose appropriate values for the phenomenological parameter ϵ , we have performed a series of simulation tests in the interval $1.0 \leq \epsilon \leq 5.0$, which includes and partially extends the range of ϵ used in several works on self-assembly of different amphiphilic systems.^{51,67,69–74} At low ϵ , aggregates are quite rare and only isolated ACDs exist, whereas a high value of ϵ strongly reduces the motion of the molecules and generally leads the system toward a phase separation. In the following, only systems with ϵ between 1.67 and 2.5, which show a richer and more intriguing aggregation behavior, are analyzed.

The bonded interactions complete the functional form of the force field. They incorporate two energy terms describing the fluctuations of the bond length and angle. Both terms are modeled by harmonic potentials of the form

$$U_{\text{VIB}} = K_{\text{angle}}[\cos(\theta) - \cos(\theta_0)]^2 + K_{\text{bond}}(l - l_0)^2 \quad (3)$$

where U_{VIB} is the potential energy resulting from the fluctuations of the bond length (l) and angle (θ) around their equilibrium values $l_0 = \sigma$ and $\theta_0 = \pi$, respectively. K_{angle} and K_{bond} are force constants whose values determine the most probable bond length and bending properties (stiffness) of all the chains. In all the simulations, we set $K_{\text{angle}} = 0.2\epsilon \text{ rad}^{-2}$ and $K_{\text{bond}} = 1000\epsilon\sigma^{-2}$ to prevent large bond stretching. These parameters have been fixed in the range of those generally proposed for self-assembling amphiphilic systems.^{51,70,72} Although their effect on the aggregation behavior of ACDs is not particularly significant, we are currently considering to investigate it in detail in a future work.

III. SIMULATION METHODOLOGY

We have performed off-lattice MC simulations in the canonical ensemble, where the total number of beads, the box area, and the temperature are kept constant. Periodic boundary conditions have been applied and the cell list (or linked list) method was implemented.^{75,76} The systems studied have different packing fractions, ranging from $\phi = 0.20$ to 0.70 , but the same temperature ($T = 300$ K) and box area ($A/\sigma^2 = 100\text{-}100$). The packing fraction is defined as $\phi = Na_0/A$, where a_0 is the area occupied by a single ACD molecule. The number of ACD molecules ranges between 60 and 211, depending on the packing fraction of the system. At $\phi = 0.20$, simulations in big boxes with area $A/\sigma^2 = 300\text{-}300$ have also been run in order to check the occurrence of eventual finite size effects. In these cases, the total number of molecules was 540. In all the simulations, the starting configurations consisted of molecules of ACDs sequentially placed in a lattice-like fashion, which were allowed to relax at a very high temperature. This created a

completely random distribution of the ACDs and the starting configuration for the simulation runs.

The MC moves performed here are of three general kinds: simultaneous moves of several molecules, simultaneous moves of all the beads belonging to a given molecule, and moves of (a part of) a selected chain. The first group of moves consist of cluster moves. By cluster, we mean a group of molecules sharing at least one bead belonging to any lipophilic tail. Because of the significant computational effort implied to perform cluster moves, they are attempted only at low-to-moderate packing fractions, where the acceptance probability is not vanishing. The second group of moves consist of displacements and rotations. The maximum elementary displacement, δl_{\max} and rotation, $\delta\theta_{\max}$ are fixed in order to give an acceptance rate of roughly 30%. Rotations can take place around any of the N beads of a model ACD, which is randomly selected as the center of rotation of the whole molecule. Displacements and rotations can be performed separately or together. Finally, configurational bias moves have been implemented to attempt the partial or complete regrowth of a hydrophilic or lipophilic chain. Beads of the trapezoidal cavity are never selected to perform bias moves. According to the scheme proposed by Frenkel and Smit, we first generate a trial configuration and calculate the corresponding Rosenbluth weight, W_R^{trial} , and then we consider the old configuration with its Rosenbluth weight, W_R^{old} .⁷⁵ The move is accepted with probability

$$\Pi = \min[1, W_R^{\text{trial}}/W_R^{\text{old}}] \quad (4)$$

To compute W_R^{trial} , a finite number of trial orientations must be generated. In a lattice model, this number cannot be larger than the lattice coordination number, whereas in an off-lattice model, there are infinite possible random orientations. Clearly, it is computationally convenient to calculate the Rosenbluth weight just for a restricted number of trial orientations. We chose $k = 10$, being a good compromise between the computational time required for each attempted move and the percentage of accepted moves.

The types of move were selected randomly. At packing fractions above $\phi = 0.50$, we used a 25% probability for displacement, rotation, simultaneous displacement and rotation, and configurational bias moves. No cluster moves were performed at these dense packings. At $\phi < 0.50$, the probability of attempting a bias move has been decreased to 20%, and, accordingly, the probability to perform cluster moves increased up to 5%. Simulations are considered finished if the total energy of the system has reached a steady value within its statistical fluctuations, as exemplarily shown in Figure 2, where the total energy of some systems studied here is given as a function of the MC cycles. The abrupt jumps observed in the system with $\phi = 0.40$ and $\epsilon = 2.5$ (brown curve) are due to successful cluster moves.

At the end of the equilibration run, the cluster size distribution, density distribution profile, and the radial distribution function are computed. The cluster size distribution estimates the average preferential size of the micellar aggregates and their dispersion in solution. Following the criterion used in previous works,^{57,60} an aggregate (or cluster) is defined as an assembly of ACD molecules sharing at least one L bead as a neighbor. More specifically, the cluster size distribution, $P(n)$, represents

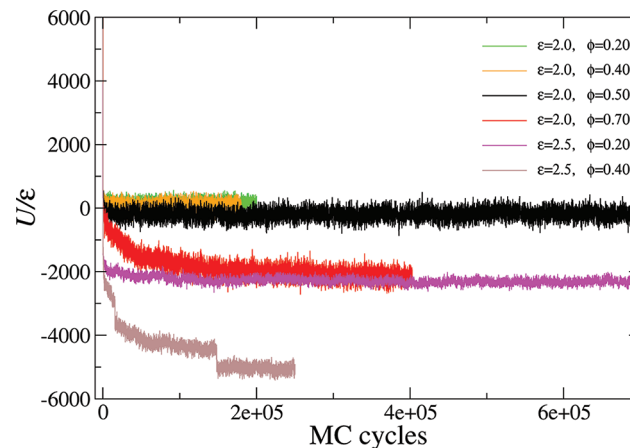


Figure 2. Total energy, in units of ϵ , of some systems studied in this paper as a function of MC cycles. In the legend, the interaction strength ϵ and packing fractions ϕ are given. The abrupt jumps observed in the system with $\phi = 0.40$ and $\epsilon = 2.5$ are due to successful cluster moves.

the average fraction of clusters of size n observed in the equilibrated system during the production run. It reads

$$P(n) = \frac{\langle \psi_n \rangle}{nN/A} \quad (5)$$

where $\langle \psi_n \rangle$ is the average concentration of clusters that contain n molecules consisting of N beads and A is the area of the simulation box.

The (normalized) density distribution profile, $\rho_j(r)$, of a given bead j was defined as

$$\rho_j(r) = \frac{\langle \rho_j(r) \rangle}{\rho_j} \quad (6)$$

where $\langle \rho_j(r) \rangle$ is the average local density of beads j in the r direction for a given structure, using as the origin the center of that structure, whereas $\rho_j = N_j/A$ is the density of the total number of beads of type j , N_j , in the simulation box. To compute a density profile, one should specify the structural arrangement of the aggregate. For circular aggregates, it is convenient to calculate $\rho_j(r)$ at concentric shells around the center of mass of the aggregate. When lamellar structures are formed, one locates a plane at the center of the lipophilic core of a given smectic layer, and $\rho_j(r)$ is obtained in the perpendicular direction to that plane.

In some cases, it is not straightforward to define a structure that would allow to determine the density distribution profiles. However, it is still possible to detect lipophilic or hydrophilic domains. To overcome this problem, the radial distribution function, which does not imply the assumption of any particular structure, can be computed. In particular, the radial distribution function, $g_{ij}(r)$, correlates the local composition around a bead of type i , with the overall composition of beads of type j :

$$g_{ij}(r) = \frac{1}{\rho_j} \frac{\langle N_j(r) \rangle_i}{A(r)} \quad (7)$$

where $\langle N_j(r) \rangle_i$ is the average number of beads of type j at a distance r from a site of type i and $A(r)$ is the area of the shell of radius r and center in i .

IV. RESULTS

As observed in section II, at relatively low values of ϵ , the aggregation of the ACDs is quite poor and the molecules tend to persist in their isolated state. In Figure 3a, a snapshot of the

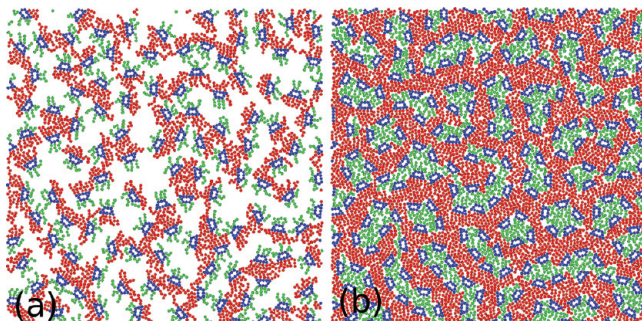


Figure 3. Snapshots of systems containing ACDs at $T = 300$ K, $\epsilon = 1.67$, and packing fractions $\phi = 0.40$ (a) and 0.70 (b). Box area: $A/\sigma^2 = 100 \times 100$. The hydrophilic and lipophilic chains consist of green and red beads, respectively. The hard central cavity is represented by blue beads.

system with $\epsilon = 1.67$ and packing fraction $\phi = 0.40$ confirms this behavior, which is directly due to the weak attractions between the lipophilic chains of ACD molecules. More precisely, the $L-L$ attractions are such that the short-ranged intermolecular repulsions between the hydrophilic H beads can partially balance them, thus fading away the driving force for the self-aggregation of ACDs. This situation is analogous to that of a system containing a solvent, such as methanol, whose modest polar character would result in a weak attraction between the L beads, making the formation of aggregates less probable. If the packing fraction is increased up to $\phi = 0.70$, the simulation box is almost completely occupied by amphiphilic molecules. In this context, we observe the formation of irregular size and shaped polydispersed aggregates which show a hydrophilic core and are completely surrounded by a sea of lipophilic beads. The arrangement stemming from this configuration might be regarded as a weakly ordered bicontinuous or inverted micellar phase, where roughly circular and stringlike aggregates are simultaneously detected.

When the value of ϵ increases, that is when the polarity of the solvent becomes high enough to induce stronger attractions between L beads, a richer and more interesting self-assembly is observed. In Figures 4 and 5, we give some visual samples of the aggregation behavior of ACDs at different packing fractions, between $\phi = 0.20$ and 0.70 , and $\epsilon = 2$. In Figure 4a,b, the initial and final configurations of the system at $\phi = 0.20$ are shown separately in a big simulation box with area $A/\sigma^2 = 300 \times 300$.

At $\phi = 0.20$, isolated molecules and small clusters are simultaneously observed. Such clusters are predominantly formed by three molecules, although bigger aggregates are sometimes detected, as it is corroborated by the cluster size distribution given in the inset of Figure 6. Small aggregation numbers have also been determined for micellar aggregates observed experimentally in systems of nonionic ACDs.³¹ In the mainframe of the same figure, we compare the local composition around an L bead, with the overall composition of beads of type L , H , or C , by computing the radial distribution functions g_{LL} , g_{LH} , and g_{LC} , respectively. At short distances, where g_{LL} is much larger than unity, the L beads are almost completely surrounded by other L beads, indicating the presence

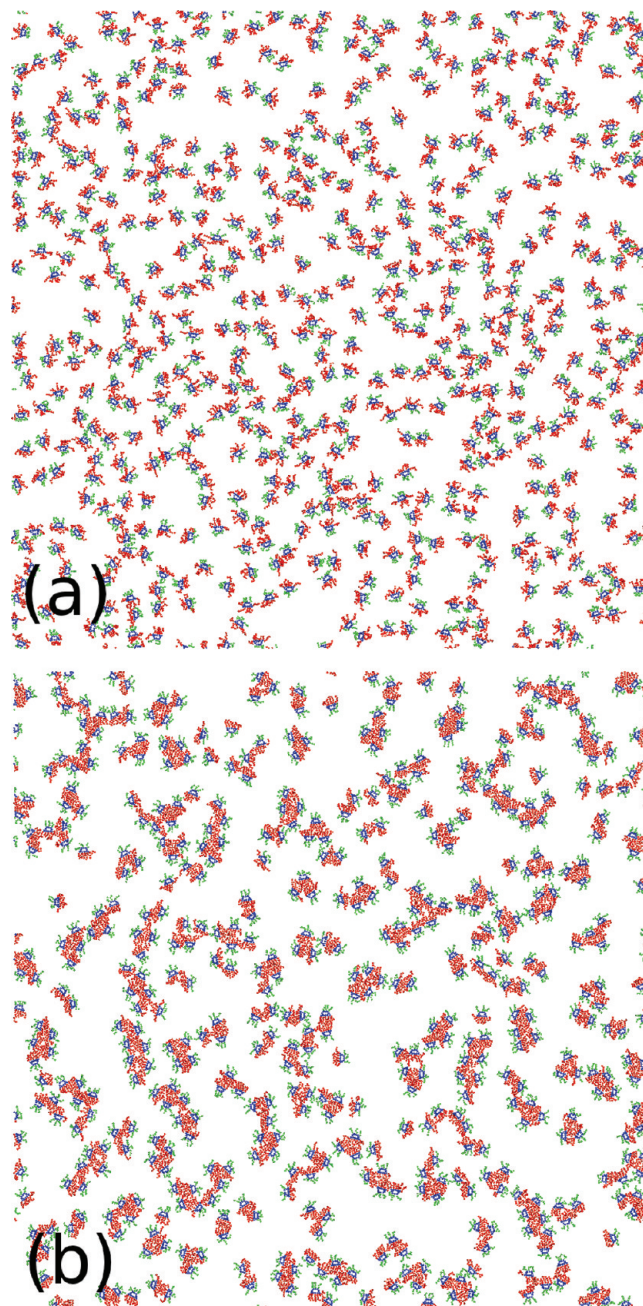


Figure 4. Initial (a) and final (b) configurations of the system containing 540 ACDs at $T = 300$ K, $\epsilon = 2$, and $\phi = 0.20$. Area of the simulation box: $A/\sigma^2 = 300 \times 300$. The hydrophilic and lipophilic chains consist of green and red beads, respectively. The central cavity is represented by blue beads.

of lipophilic-rich domains. Since the fluctuations of g_{LL} decay to one at a distance of roughly 8σ from the core of such domains, we conclude that the aggregates do not form long-range ordered structural correlations but behave as isolated objects in a fluid-like phase. A similar behavior is observed for the g_{LC} distribution, where the correlations between L and C beads are limited to a radial distance enwrapping a single aggregate and decay to one just beyond it. Therefore, the C beads are in the proximity of L beads, but they do not mix at short distances. The remaining radial distribution function, g_{LH} , unveils a very weak correlation between H and L beads, with values much lower than one at short distances and a quite broad peak at $r \simeq 6\sigma$. In other words,

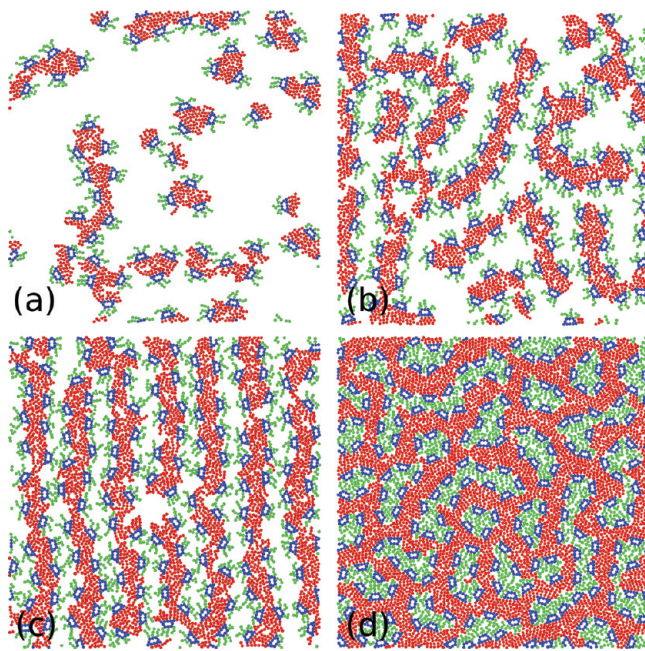


Figure 5. Snapshots of systems containing ACDs at $T = 300\text{ K}$, $\epsilon = 2$, and packing fractions $\phi = 0.20$ (a), 0.40 (b), 0.50 (c), and 0.70 (d). Box area: $A/\phi^2 = 100 \times 100$. The hydrophilic and lipophilic chains consist of green and red beads, respectively. The central cavity is represented by blue beads.

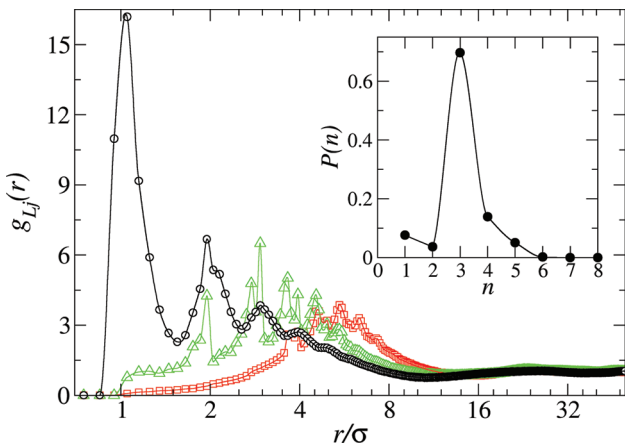


Figure 6. Radial distribution functions (g_{Lj}) of the system containing ACDs at $T = 300\text{ K}$, $\epsilon = 2$, and $\phi = 0.20$. The black circles, red squares, and green triangles, refer to the g_{LL} , g_{LH} , and g_{LC} radial distribution functions, respectively. Note the logarithmic scale of the horizontal axis. In the inset, the cluster size distribution is given. The solid lines in the main frame as well as that in the inset are a guide for the eyes.

H beads are not likely to be mixed with the L beads, as confirmed by visual inspection of the snapshot given in Figure 5a. At longer distances, we find again the typical features of a fluidlike behavior, with an exponential decay of the oscillations to one at $r > 8\sigma$.

By increasing the packing fraction to 0.40, it is still possible to notice few small clusters containing three or four molecules, but the formation of relatively long aggregates becomes more and more evident. The structural nature of these elongated and thin clusters can be described as two connected filaments of side-linked molecules separating and hence protecting the lipophilic groups from the contact with the hydrophilic ones.

The arrangement of the ACDs in these stringlike clusters produces a quite regular pattern tracing a zigzag path between the two parallel filaments, as clearly indicated in Figure 7.

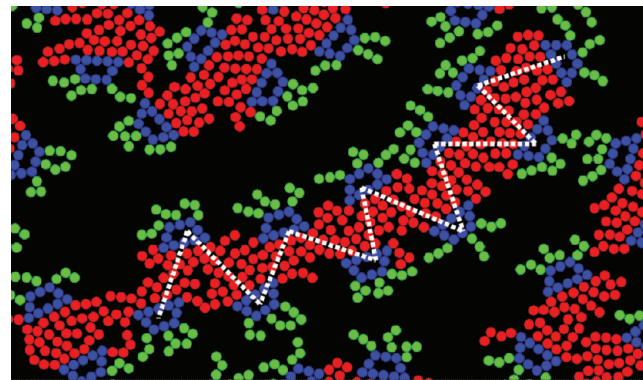


Figure 7. Detail of the zigzag (interdigitated) arrangement in a stringlike cluster containing ACDs. $\phi = 0.40$ and $\epsilon = 2$. The white dashed lines are a guide for the eyes.

Interestingly enough, this characteristic configuration had previously been postulated in an experimental study on nonionic bilayer vesicles of ACDs, where the lipophilic chains, as well as their respective cavities, were shown to be deeply interdigitated,⁷⁷ in a similar fashion to that observed in asymmetric phospholipids⁷⁸ and amphiphilic calixarenes.⁷⁹ By using small-angle X-ray diffraction and pressure-area isotherms, it was demonstrated that the bilayer thickness depends on the interdigitation between the alkyl chains. Because of this special arrangement, which implies a dense layer packing, the mobility of the hydrocarbon chains result to be significantly reduced as well as the possibility to observe interlayer leaks.

One can better appreciate this peculiar aggregation behavior at higher packing fractions. At $\phi = 0.50$, the filamentous clusters become the preferred state of aggregation, being other kinds of clusters or isolated molecules virtually absent. In this context, we also note a remarkable change in the long-range self-assembly of our system. More specifically, the filamentous clusters stop behaving as isolated objects to form a 2D macroscopic structure with a higher degree of order. Despite the distinctive presence of defects, we can clearly distinguish the tendency to determine a 2D smectic liquid crystalline phase, consisting of stacks of fluidlike filaments of orientationally ordered ACDs. In Figure 8, the normalized density distribution profiles of L , H , and C beads in the direction normal to the layers are given. The peaks of density in the three distribution profiles confirm the periodical accumulation of these beads from a layer to another. The peaks of the L profiles are located where the minima of the H density curves are found; namely, they are out of phase with each other, indicating that it is very rare to observe hydrophilic beads inside the lipophilic core of the smectic liquid crystal phase. As far as the C beads are concerned, their density distribution profiles show a twice as high frequency as that of the other two profiles, with peaks located at an intermediate distance between the lipophilic and hydrophilic cores. The distance between two consecutive peaks in the $\rho_L(r)$ distribution gives a measure of the average distance between two neighboring layers, which is approximately $r/\sigma = 15$. Because of the presence of the ACD cavities, which do not take part to the self-assembly process and thus remain available for the encapsulation of suitable molecular

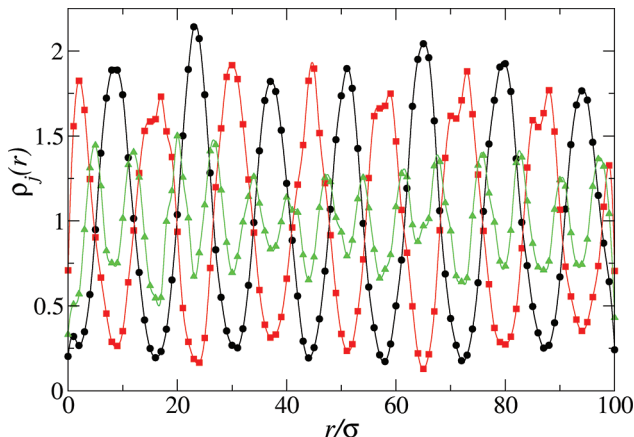


Figure 8. Density distribution profiles of lipophilic (black circles), hydrophilic (red squares), and cavity beads (green triangles), in the system containing ACDs at $T = 300\text{ K}$, $e = 2$, and $\phi = 0.50$, calculated along the direction perpendicular to the smectic layers. The solid lines are a guide for the eyes.

guests, this ordered layered architecture provides a favorable environment to prepare functional nanostructured materials with homogeneous distribution of active sites. Sortino and co-workers have recently investigated the synthesis of photo-responsive nanomaterials made of hybrid layers of ACDs and hydrophilic porphyrins.^{80,81} They pointed out the possibility to promote a light-controlled transport of electrons between appropriate incorporated guests and the porphyrin molecules to produce more sofisticated supramolecular structures for targeted applications, such as photodynamic therapy of tumor cells.

At $\phi = 0.70$, due to the high content of molecules, a distinct scenario emerges. We note the formation of roughly circular or slightly elongated dominia showing an inner hydrophilic core and completely surrounded by a continuous and dense network of lipophilic chains. The radial distribution functions of this system, g_{HH} , g_{HL} and g_{HC} given in Figure 9, suggest that the H

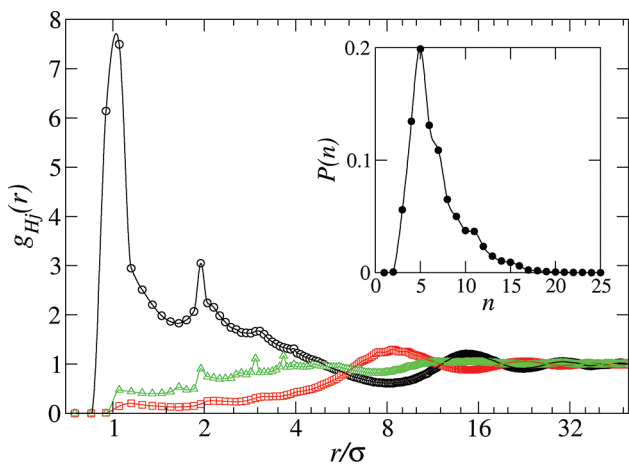


Figure 9. Radial distribution functions (g_{HH}) of the system containing ACDs at $T = 300\text{ K}$, $e = 2$, and $\phi = 0.70$. The black circles, red squares, and green triangles, refer to the $H-H$, $H-L$, and $H-C$ radial distribution functions, respectively. Note the logarithmic scale of the horizontal axis. In the inset, the cluster size distribution is given. The solid lines in the main frame as well as that in the inset are a guide for the eyes.

beads are mostly surrounded by other H beads, being the L beads clearly separated from them. The phase that we are detecting consists of an inverted micellar structure, which spontaneously forms at very high packing fractions to optimize the packing of the molecules and hence to minimize the total intermolecular energy. The $H-H$ correlations persist beyond the radius enclosing a single aggregate and another evident peak at roughly $r = 15\sigma$ is detected. The distance between this peak and the first one in the g_{HH} can be used as a measure of the average distance between the core of two neighboring micellar aggregates. Furthermore, the shape of the g_{HL} distribution (red squares in Figure 9), whose first peak coincides with the first minimum of g_{HH} , points out the segregation between H and L beads. As a matter of fact, at short distances, the g_{HL} distribution is quite smaller than unity, indicating that the H beads are not likely to be mixed with the L beads. In the inset of Figure 9, the cluster size distribution is provided. In this case, a cluster is an ensemble of molecules sharing at least an H bead, instead of an L bead, as a neighbor, similarly to the above definition for direct aggregates. Accordingly, the peak of the distribution indicates the most probable size of aggregates with a hydrophilic core, which is $n \approx 5$. This distribution results to be substantially broader than that given in Figure 6, suggesting the simultaneous presence of polydispersed hydrophilic cores. In some cases, small clusters of few ACDs may join together and form bigger aggregates, as detected by visual inspection of Figure 5d and confirmed by the long tail of the cluster size distribution in the inset of Figure 9.

In order to investigate the effects of a highly polar surrounding media, such as pure water or aqueous mixtures with a high content of water,⁸² on the aggregation behavior of ACDs, the phenomenological parameter is increased up to $e = 2.5$. Under such conditions, the interactions established between pairs of lipophilic beads become highly attractive, and the presence of isolated molecules very unlikely, even at low packing fractions. In Figure 10,

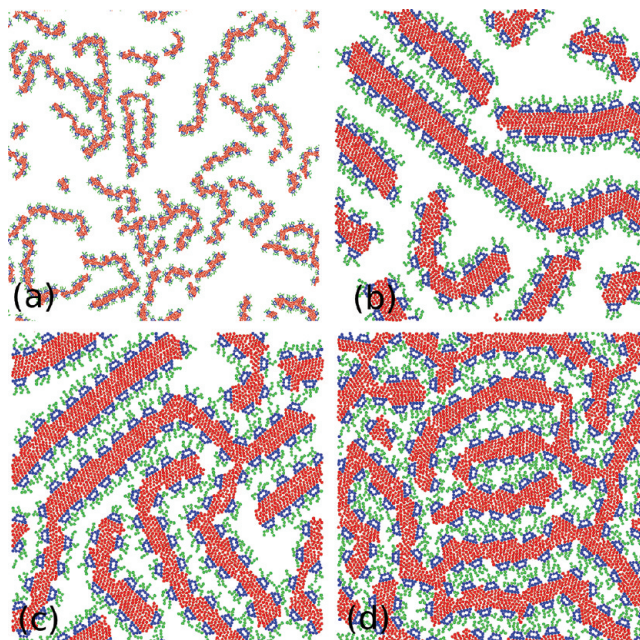


Figure 10. Snapshots of systems containing ACDs at $T = 300\text{ K}$, $e = 2.5$, and packing fractions $\phi = 0.20$ (a), 0.40 (b), 0.50 (c), and 0.60 (d). At $\phi = 0.20$, the box area is $A/\sigma^2 = 300 \times 300$, whereas at the remaining packing fractions $A/\sigma^2 = 100 \times 100$. The hydrophilic and lipophilic chains consist of green and red beads, respectively. The central cavity is represented by blue beads.

some typical configurations of systems at $\epsilon = 2.5$ and different packing fractions are exemplarily shown. Already at $\phi = 0.20$, stringlike clusters of side-linked molecules are formed. This leads to a drastic reduction of the exposure of the lipophilic chains to the surrounding media as compared to systems with the same packing fraction and lower interaction strength, such as that observed in Figure 5a. These filamentous aggregates are very similar to those observed in Figures 5b and 5c at $\phi = 0.40$ and 0.50, respectively. However, due to the significant strength of attraction between L-type beads, the inner density of such clusters results to be higher as well as their average stiffness. This result is especially evident in the systems at the highest packing fractions, that is from $\phi = 0.40$ up to 0.60, given in Figure 10b–d. At $\phi = 0.50$, we determine a significantly different morphology as compared to the long-range ordered smectic phase detected, in Figure 5c, at the same packing fraction and lower interaction parameter ($\epsilon = 2$). More specifically, the stringlike clusters of Figure 10 are more compact than those of Figure 5, hence suggesting a higher inertia toward structural fluctuations and, consequently, in self-healing eventual structural defects. The resulting configuration no longer presents a liquid crystalline aspect, but instead it looks like a colloidal gel network of heterogeneous stringlike clusters. At $\phi = 0.20$ (see Figure 10a), thanks to the lower concentration of surrounding stringlike aggregates, the filaments can achieve longer extensions and thus more easily bend to form circular structures.

As a general tendency, regardless the packing fraction, the filaments can (i) meet and form branched structures and/or (ii) bend and give rise to curved domains. In some cases, a combination of both arrangements is also observed. Branched arrangements are usually Y-shaped clusters, being three filaments of various length converging at a given point. By contrast, curved filaments have more heterogeneous geometrical characteristics. In some cases, they appear like weakly ordered open circles, which, being thermodynamically unstable because of the unshielded lipophilic beads at both ends, tend to join together or close on themselves to form circular double-layered aggregates. Although their structural features should be addressed in more detail, such aggregates would denote the tendency of ACDs to form vesicles. In Figure 10, at $\phi = 0.50$ and 0.60, and especially at $\phi = 0.20$, one can easily detect few circular aggregates with one or more filaments sticking out from them. Most probably, these systems are stuck in energy minima that dramatically increase the computational time to achieve a full equilibration and thus delay the formation of conventional vesicles observed in experiments.⁸³

V. CONCLUSIONS

In summary, we have studied the self-aggregation behavior of coarse-grained ACDs by performing off-lattice MC simulations of a 2D implicit-solvent model. Suppressing the solution degrees of freedom and constraining the ACDs to rotate and translate in a 2D space imply a substantial simplification of the real system but, at the same time, drastically reduce its complexity and thus offer the possibility to investigate and understand the main ingredients affecting the ACDs self-assembly. The interaction between the amphiphilic molecules and the solvent is implicitly considered in the phenomenological parameter of our model, that is, ϵ . By tuning this parameter, which measures the strength of interaction between the hydrocarbon chains, an intriguing self-assembly behavior has been determined. More specifically, at low values of ϵ , intermolecular aggregation is very poor as the repulsion between the hydrophilic chains dominates over the

attraction between the lipophilic chains, thus leading to an isotropic phase of isolated ACDs. In this case, no significant clusters form and even dimers are quite rare. When the interaction strength increases, an intriguing scenario consisting of circular as well as elongated micellar aggregates, stringlike clusters, lamellar, and inverted micellar phases was found and investigated. The computation of cluster size distribution and radial distribution function allowed the characterization of the micellar structures observed, which generally show an aggregation number of few units of molecules and a relatively weak correlation at long distances, typically detected in amphiphilic systems above the critical micellar concentration. Many structural characteristics, such as the molecular interdigititation in the bilayer strings and the formation of a long-ranged ordered smectic phase, show a surprisingly good qualitative agreement with the aggregation behavior reported in experimental works.

■ AUTHOR INFORMATION

Corresponding Author

*E-mail: alessandro.patti@iqac.csic.es.

Notes

The authors declare no competing financial interest.

■ ACKNOWLEDGMENTS

A.P. acknowledges a Beatriu de Pinós postdoctoral grant from Generalitat de Catalunya (2009BP-B00058) and the computational resources offered by The Centre de Serveis Científics i Acadèmics de Catalunya (CESCA). This work has also been supported by grant 2009-SGR-961 from Generalitat de Catalunya.

■ REFERENCES

- (1) Villiers, A. *C. R. Fr. Acad. Sci.* **1891**, *112*, 435–438.
- (2) Loftsson, T.; Brewster, M. *E. J. Pharm. Sci.* **1996**, *85*, 1017–1025.
- (3) Loftsson, T.; Duchêne, D. *Int. J. Pharm.* **2007**, *329*, 1–11.
- (4) Ma, M.; Li, D. *Chem. Mater.* **1999**, *11*, 872–874.
- (5) Bibby, A.; Mercier, L. *Green Chem.* **2003**, *5*, 15–19.
- (6) Mamba, B. B.; Krause, R. W.; Malefetse, T. J.; Nxumalo, E. N. *Environ. Chem. Lett.* **2007**, *5*, 79–84.
- (7) Mhlanga, S. D.; Mamba, B. B.; Krause, R. W.; Malefetse, T. J. *J. Chem. Technol. Biotechnol.* **2007**, *82*, 382–388.
- (8) Astraya, G.; Gonzalez-Barreiro, C.; Mejutoa, J. C.; Rial-Oterob, R.; Simal-Gándara. *J. Food Hydrocolloids* **2009**, *23*, 1631–1640.
- (9) Tarimci, N. *Cyclodextrins in the Cosmetic Field*. In Bilensoy, E., Ed.; *Cyclodextrins in Pharmaceutics, Cosmetics, and Biomedicine: Current and Future Industrial Applications*; John Wiley and Sons: New York, 2011.
- (10) Szejtli, J. *Chem. Rev.* **1998**, *98*, 1743–1754.
- (11) Saenger, W.; Jacob, J.; Gessler, K.; Steiner, T.; Hoffmann, D.; Sanbe, H.; Koizumi, K.; Smith, S. M.; Takaha, T. *Chem. Rev.* **1998**, *98*, 1787–1802.
- (12) Lipkowitz, K. B. *Chem. Rev.* **1998**, *98*, 1829–1874.
- (13) Uekama, K.; Hirayama, F.; Irie, T. *Chem. Rev.* **1998**, *98*, 2045–2076.
- (14) Perret, F.; Parrot-Lopez, H. *Amphiphilic Cyclodextrins: Synthesis and Characterization*. In Bilensoy, E., Ed.; *Cyclodextrins in Pharmaceutics, Cosmetics, and Biomedicine: Current and Future Industrial Applications*; John Wiley and Sons: New York, 2011.
- (15) Roux, M.; Perly, B.; Djedaini-Pillard, F. *Eur. Biophys. J.* **2007**, *36*, 861–867.
- (16) Connors, K. A. *Chem. Rev.* **1997**, *97*, 1325–1357.
- (17) Wenz, G. *Angew. Chem., Int. Ed. Engl.* **1994**, *33*, 803–822.
- (18) Khan, A. R.; Forgo, P.; Stine, K. J.; D’Souza, V. T. *Chem. Rev.* **1998**, *98*, 1977–1996.

- (19) Méndez-Ardoy, A.; Gómez-García, M.; Ortiz Mellet, C.; Sevillano, N.; Girón, M. D.; Salto, R.; Santoyo-González, F.; García Fernández, J. M. *Org. Biomol. Chem.* **2009**, *7*, 2681–2684.
- (20) Bellanger, N.; Perly, B. *J. Mol. Struct.* **1992**, *273*, 215–226.
- (21) Lin, J.; Creminon, C.; Perly, B.; Djedaini-Pilard, F. *J. Chem. Soc., Perkin Trans. 1* **1998**, *2*, 2639–2646.
- (22) Liu, F. Y.; Kildsig, D. O.; Mitra, A. K. *Drug Dev. Ind. Pharm.* **1992**, *18*, 1599–1612.
- (23) Kawabata, Y.; Matsumoto, M.; Tanaka, M.; Takahashi, H.; Irinatsu, Y.; Tamura, S.; Tagaki, W.; Nakahara, H.; Fukuda, K. *Chem. Lett.* **1986**, *1*, 1933–1934.
- (24) Cancell, J.; Jullien, L.; Lacombe, L.; Lehn, J.-M. *Chim. Acta* **1992**, *75*, 791–812.
- (25) Wenz, G. *Carbohydr. Res.* **1991**, *214*, 257–265.
- (26) Lesieur, S.; Charon, D.; Lesieur, P.; Ringard-Lefebvre, C.; Muguet, V.; Duchêne, D.; Wouessidjewe, D. *Chem. Phys. Lipids* **2000**, *106*, 127–144.
- (27) Zhang, P.; Ling, C. C.; Coleman, A. W.; Parrot-Lopez, H.; Galons, H. *Tetrahedron Lett.* **1991**, *32*, 2769–2770.
- (28) Zhang, P.; Parrot-Lopez, H.; Tchoreloff, P.; Baszkin, A.; Ling, C. C.; De Rango, C.; Coleman, A. W. *J. Phys. Org. Chem.* **1992**, *5*, 518–528.
- (29) Duchêne, D.; Wouessidjewe, D.; Ponchel, G. *J. Controlled Release* **1999**, *62*, 263–268.
- (30) Lin, J.; Djedaini-Pilard, F.; Perly, B. French Patent 95 07841/1995.
- (31) Lombardo, D.; Longo, A.; Darcy, R.; Mazzaglia, A. *Langmuir* **2004**, *20*, 1057–1064.
- (32) Winkler, R. G.; Fioravanti, S.; Ciccotti, G.; Margheritis, C.; Villa, M. *J. Comput.-Aided Mol. Des.* **2000**, *14*, 659–667.
- (33) Lawtrakul, L.; Viernstein, H.; Wolschann, P. *Int. J. Pharm.* **2003**, *256*, 33–41.
- (34) Georg, H. C.; Coutinho, K.; Canuto, S. *Chem. Phys. Lett.* **2005**, *413*, 16–21.
- (35) Taulier, N.; Chalikian, T. V. *J. Phys. Chem. B* **2006**, *110*, 12222–12224.
- (36) Raffaini, G.; Ganazzoli, F. *Chem. Phys.* **2007**, *333*, 128–134.
- (37) Maestre, I.; Bea, I.; Ivanov, P. M.; Jaime, C. *Theor. Chem. Acc.* **2007**, *117*, 85–97.
- (38) Heine, T.; Dos Santos, H. F.; Patchkovskii, S.; Duarte, H. A. *J. Phys. Chem. A* **2007**, *111*, 5648–5654.
- (39) Cai, W.; Sun, T.; Shao, X.; Chipot, C. *Phys. Chem. Chem. Phys.* **2008**, *10*, 3236–3243.
- (40) Boonyarattanakalin, K. S.; Wolschann, P.; Lawtrakul, L. *J. Inclusion Phenom. Macrocyclic Chem.* **2011**, *70*, 279–290.
- (41) Ding, J.; Steiner, T.; Zabel, V.; Hingerty, B. E.; Mason, S. A.; Saenger, W. *J. Am. Chem. Soc.* **1991**, *113*, 8081–8089.
- (42) Fujiwara, T.; Tanaka, N.; Kobayashi, S. *Chem. Lett.* **1990**, *19*, 739.
- (43) Cézard, C.; Trivelli, X.; Aubry, F.; Djedaini-Pilard, F.; Dupradeau, F.-Y. *Phys. Chem. Chem. Phys.* **2011**, *13*, 15103–15121.
- (44) Saenger, W.; Betzel, Ch.; Hingerty, B.; Brown, G. M. *Nature (London)* **1982**, *296*, 581–583.
- (45) Sellner, B.; Zifferer, G.; Kornherr, A.; Krois, D.; Brinker, U. H. *J. Phys. Chem. B* **2008**, *112*, 710–714.
- (46) Raffaini, G.; Ganazzoli, F.; Malpezzi, L.; Fuganti, C.; Fronza, G.; Panzeri, W.; Mele, A. *J. Phys. Chem. B* **2009**, *113*, 9110–9122.
- (47) Zhang, H.; Feng, W.; Li, C.; Tan, T. *J. Phys. Chem. B* **2010**, *114*, 4876–4883.
- (48) Brocos, P.; Díaz-Vergara, N.; Banquy, X.; Pérez-Casas, S.; Costas, M.; Piñeiro, Á. *J. Phys. Chem. B* **2010**, *114*, 12455–12467.
- (49) Wang, T.; Chipot, C.; Shao, X.; Cai, W. *Langmuir* **2010**, *27*, 91–97.
- (50) Hernández-Pascacio, J.; Garza, C.; Banquy, X.; Díaz-Vergara, N.; Amigo, A.; Ramos, S.; Castillo, R.; Costas, M.; Piñeiro, Á. *J. Phys. Chem. B* **2007**, *111*, 12625–12630.
- (51) Bhattacharya, A.; Mahanti, S. D.; Chakrabarti, A. *J. Chem. Phys.* **1998**, *108*, 10281–10293.
- (52) Panagiotopoulos, A. Z.; Floriano, M. A.; Kumar, S. K. *Langmuir* **2002**, *18*, 2940–2948.
- (53) Kim, S. Y.; Panagiotopoulos, A. Z.; Floriano, M. A. *Mol. Phys.* **2002**, *100*, 2213–2220.
- (54) Siperstein, F. R.; Gubbins, K. E. *Langmuir* **2003**, *19*, 2049–2057.
- (55) Bhattacharya, S.; Gubbins, K. E. *J. Chem. Phys.* **2005**, *123*, 134907.
- (56) Jorge, M.; Auerbach, S. M.; Monson, P. A. *J. Am. Chem. Soc.* **2005**, *127*, 14388–14400.
- (57) Patti, A.; Mackie, A. D.; Siperstein, F. R. *Langmuir* **2007**, *23*, 6771–6780.
- (58) Cui, J.; Jiang, W. *Langmuir* **2011**, *27*, 10141–10147.
- (59) Gemma, T.; Hatano, A.; Dotera, T. *Macromolecules* **2002**, *35*, 3225–3237.
- (60) Patti, A. *Colloids Surf., A* **2010**, *361*, 81–89.
- (61) Song, J.; Shi, T.; Chen, J.; An, L. *J. Phys. Chem. B* **2010**, *114*, 16318–16328.
- (62) Martsinovich, N.; Troisi, A. *J. Phys. Chem. C* **2010**, *114*, 4376–4388.
- (63) Klos, J. S.; Sommer, J.-U. *J. Chem. Phys.* **2011**, *134*, 204902.
- (64) Smit, B.; Esselink, K.; Hilbers, P. A.; van Os, N. M.; Rupert, L. A. M.; Szleifer, I. *Langmuir* **1993**, *9*, 9–11.
- (65) Palmer, B.; Liu, J. *Langmuir* **1996**, *12*, 6015–6021.
- (66) Maiti, P. K.; Lansac, Y.; Glaser, M. A.; Clark, N. A. *Langmuir* **2002**, *18*, 1908–1918.
- (67) Shi, Z.; Chen, N.; Du, Y.; Khademhosseini, A.; Alber, M. *Phys. Rev. E* **2009**, *80*, 061901.
- (68) Samanta, S. K.; Bhattacharya, S.; Maiti, P. K. *J. Chem. Phys.* **2009**, *113*, 13545–13550.
- (69) Bourov, G. K.; Bhattacharya, A. *J. Chem. Phys.* **2003**, *119*, 9219.
- (70) Kim, K. H.; Kim, S. H.; Huh, J.; Jo, W. H. *J. Chem. Phys.* **2003**, *119*, 5705.
- (71) Wang, Z.-J.; Frenkel, D. *J. Chem. Phys.* **2005**, *122*, 234711.
- (72) Bourov, G. K.; Bhattacharya, A. *J. Chem. Phys.* **2007**, *127*, 244905.
- (73) Yuan, H.; Huang, C.; Li, J.; Lykotrafitis, G.; Zhang, S. *Phys. Rev. E* **2010**, *82*, 011905.
- (74) Sodt, A. J.; Head-Gordon, T. *J. Chem. Phys.* **2011**, *132*, 205103.
- (75) Frenkel, D.; Smit, B. *Understanding Molecular Simulation: From Algorithms to Applications*, 2nd ed.; Academic Press: New York, 2002.
- (76) Hockney, R. W.; Eastwood, J. W. *Computer Simulations Using Particles*; McGraw-Hill: New York, 1981.
- (77) Falvey, P.; Lim, C. W.; Darcy, R.; Revermann, T.; Karst, U.; Giesbers, M.; Marcelis, A. T. M.; Lazar, A.; Coleman, A. W.; Reinhoudt, D. N.; Ravoo, B. *J. Chem.—Eur. J.* **2005**, *11*, 1171–1180.
- (78) Seddon, J. M.; Cevc, G. In *Phospholipids Handbook*; Cevc, G., Ed.; Marcel Dekker: New York, 1993.
- (79) Shahgaldian, P.; Cesario, M.; Goreloff, P.; Coleman, A. W. *Chem. Commun.* **2002**, 326–327.
- (80) Valli, L.; Giancane, G.; Mazzaglia, A.; Monsu, L.; Sortino, S. *J. Mater. Chem.* **2007**, *17*, 1660–1663.
- (81) Sortino, S. *Photochem. Photobiol. Sci.* **2008**, *7*, 911–924.
- (82) Jiang, B.-P.; Guo, D.-S.; Liu, Y. *J. Org. Chem.* **2010**, *75*, 7258–7264.
- (83) Ravoo, B. J.; Darcy, R. *Angew. Chem.* **2000**, *112*, 4494–4496.